Rotational synchronization of pinned spiral waves

Hrishikesh Kalita, Parvej Khan, and Sumana Dutta*
Department of Chemistry, Indian Institute of Technology Guwahati, Guwahati 781039, India

(Received 20 May 2022; accepted 16 August 2022; published 2 September 2022)

Coupled rotors can spontaneously synchronize, giving rise to a plethora of intriguing dynamics. We present here a pair of spiral waves as two synchronizing rotors, coupled by diffusion. The spirals are pinned to unexcitable obstacles, which enables us to modify their frequencies and restrain their drift. In experiments with the Belousov-Zhabotinsky reaction, we show that two counterrotating spiral rotors, pinned to circular heterogeneities, can synchronize in frequency and phase. The nature of the phase synchronization varies depending on the difference in their characteristic frequencies. We observe in-phase and out-of-phase synchronization, lag synchronization, and phase resetting across the experiments. The time required for the two spirals to synchronize is found to depend upon the relative size of their pinning obstacles and the distance separating them. This distance can also modify the phase lag of the two rotors upon synchronization. Our experimental observations are reproduced and explained further on the basis of numerical simulations of an excitable reaction-diffusion model.

DOI: 10.1103/PhysRevE.106.034201

I. INTRODUCTION

The footprints of synchronization are often found in nature, like in the flashing of fireflies and chirping of crickets. They are also encountered across other diverse systems such as pendulums, clocks, lasers, and applauding audiences [1]. From population dynamics [2] to the firing of neuronal cells [3], the rhythmic nature of oscillators dictates the dynamical behavior of the system. Spontaneous synchronization is also encountered in spatially distributed oscillators in biological systems, such as the rhythmic electrochemical waves in the heart [4] or the glycolytic oscillations in suspensions of yeast cells [5]. Examples of chemical systems exhibiting synchrony are the mercury beating heart [6] and rhythmic oscillations of catalytic particles of the Belousov-Zhabotinsky (BZ) reaction [7]. The behavior of these coupled chemical and biological oscillators found a mathematical description in the seminal work of Kuramoto [8]. His model was later extended to the study of various nonidentical coupled oscillators, irrespective of the origin of the system, like Josephson junctions [9], which are superconducting rotator arrays. Ensemble of rotors, coupled electrically, mechanically, optomechanically, chemically or biologically, have been widely investigated [1,10–13]. These theoretical as well as experimental studies have revealed a wide range of rotational behavior, such as in-phase and antiphase locking [9,14], amplitude death [15], lag synchronization [13], cluster formation [12], and chimera states [16].

In this work we explore spiral waves in reaction-diffusion processes as potential candidates for the study of rotational synchronization. Spiral rotors of wave activity have been observed across various biological systems, such as cardiac tissues, retinal cells, aggregation of the social amoeba *Dictyostelium discoideum* [17], retinal [18] and uterine tissue [19], and brain cells [20]. In heart tissue, their presence can cause the disruption of coherent cardiac activity, leading to arrhythmia and life-threatening fibrillations in the atria and ventricles of the heart [21]. Spiral waves are also found in chemical systems, such as the oxidation of CO on Pt surfaces [22] and the BZ reaction [23].

Free spirals in two-dimensional spatially extended systems can trace intricate trajectories [24]. When two rigidly rotating spiral waves are initiated close to each other, they can either attract and annihilate, or repel and form bound states, depending on the distance separating them, their initial phases, and chirality of rotation [25,26]. Often, symmetry-breaking dynamics is also witnessed in such interactions. Earlier work has shown that a faster spiral wave can cause the drift of a slower one [27,28]. In order to study rotational synchronization of spirals, it is helpful to arrest the translational motion of the spiral cores. Spiral waves are known to anchor to inexcitable heterogeneities, in a process called pinning [29]. In cardiac tissues, a rotor can attach itself to a discontinuity like scar tissue, resulting in stationary rotating activity [30]. Several studies on the pinning of spiral rotors to different geometries of obstacles have been carried out [31–33]. Pinning modifies the frequency of the rotor by elongating its rotation period [34]. However, the innate nature of the spiral as a rotor remains unperturbed during the process. We propose to look at the interaction of two rigidly rotating spirals, anchored to circular disks. By varying the size of the disk, we are able to control the frequency of our rotors, enabling us to study both frequency and phase synchronization of the spiral waves. A recent numerical study explored the asymmetric interaction of arrays of pinned spiral oscillators rotating with the same frequency [35].

Here we explore the synchronization of two counterrotating pinned spiral waves, both experimentally and numerically. We carry out experiments in the BZ reaction, using

*sumana@iitg.ac.in

unexcitable circular heterogeneities of varying sizes as pinning anchors. We begin by exploring the interaction of two identical oscillators, where we find complete synchronization in frequency and phase. Changing the size of one heterogeneity, we are able to initiate two rotors with different characteristic frequencies. We then vary the distance between the two spirals and explore the changing nature of synchronization between the rotors. Numerical simulations, based on a generic reaction-diffusion model, are also carried out. These studies corroborate our experimental results while providing additional insights into the subtle dynamics of rotational motion of these reentrant excitation waves.

II. EXPERIMENTAL METHODS

Our BZ system consists of a solution of 0.16M sulfuric acid, 0.04M sodium bromate, 0.04M malonic acid, and 0.001M ferroin embedded in a 0.8 wt./vol % agar gel matrix. The solutions are prepared in Millipore water. All experiments are carried out in Petri dishes of 6 cm diameter, at room temperature ($23 \pm 1\,^{\circ}$C). The thickness of the reaction gel is maintained at around 2 mm. A plane wave is initiated in the center of the circular dish, far from the system boundaries, by inserting the tip of a silver wire into the reaction mixture for a few seconds. When the circular wave reaches the desired dimension, we cleave it with the help of a thin glass slide. The free ends of the wave now curl in to form a pair of counterrotating spiral waves. Subsequently, a chemically inert rubber cylinder, with a height equal to the thickness of the reaction layer, is placed near each tip of the spiral. The system is illuminated from below with a diffused, cold white light source and is observed by a charge-coupled device camera (mvBlueFOX 220a) mounted over it. A blue dichroic filter is used on the camera for better imaging. The images are recorded on a personal computer every 2 s and are later analyzed by using interactive, in-house MATLAB codes. The spiral tip position is recognized as the point of highest curvature touching the unexcitable disk (shown in Fig. 1).

III. EXPERIMENTAL RESULTS

Figure 1(a) shows a snapshot of a typical experiment, where the two tips of the spiral are anchored to two different-sized rubber disks of diameters d_1 and d_2. A magnified version of the area around the heterogeneities is shown in Fig. 1(b). The tips of the two spirals are located at (x_1, y_1) and (x_2, y_2), respectively, both measured in relation to the individual centers of the ith disk, with (x_{ci}, y_{ci}) considered as the origin. The distance between the centers of the circular beads is called l. The phase angles of each spiral tip with respect to the line joining the centers are denoted by θ_1 and θ_2, respectively. The motion of the pinned spiral rotor can be monitored by noting the position of the spiral tip (x_i, y_i) at any given time. The phase angle can be calculated as

$$\theta_i = \tan^{-1}\left(\frac{y_i}{x_i}\right).$$

Several experiments are carried out by changing the size of the cylinders and the distance separating them. We choose typical disk sizes of 1.8, 2.7, and 3.6 mm. It is known that a spiral anchored to an unexcitable heterogeneity moves slower than a free spiral [34]. When pinned to a cylindrical disk, the spiral core is determined by the circular perimeter of the disk, around which it rotates. Hence, larger the disk, slower should be the frequency of rotation. The time period of a free spiral (obtained with the current chemical recipe) is 10.1 min, its core diameter is 1.09 mm, and its wavelength is 9.94 mm [24]. The time periods for the pinned spiral rotors have been calculated for systems where the two spiral tips are pinned to identical obstacles (circular disks with the same diameter). For $d_1 = d_2 = 1.8$, 2.7, and 3.6 mm, the time periods are approximately $T = 12.0$, 18.0, and 24.0 min, respectively.

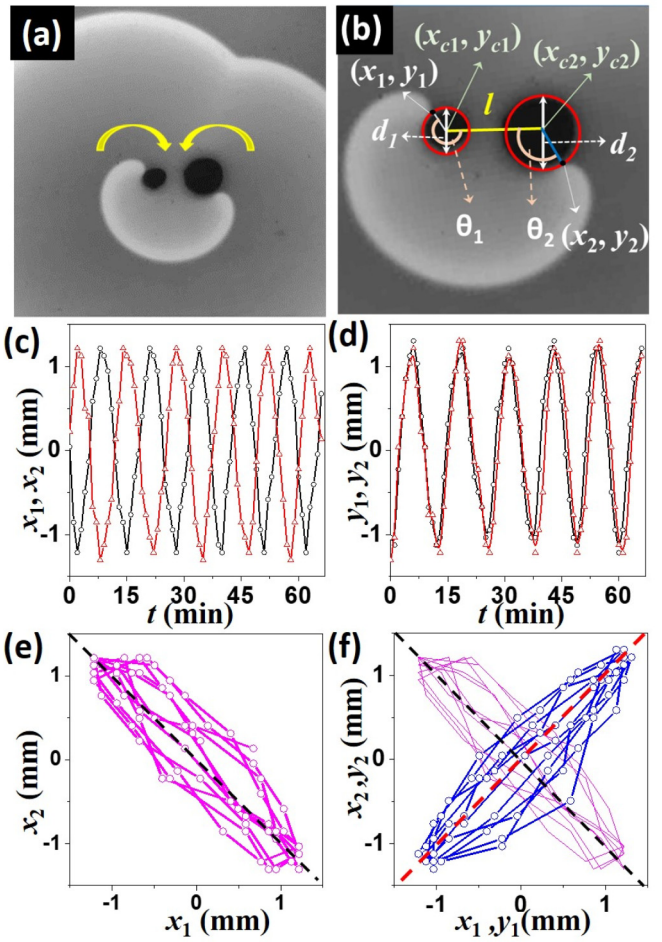

FIG. 1. Experiments to study synchronization of two pinned spiral rotors. (a) Snapshot of a typical experiment with two differently sized disks. The area of the snapshot is 30.7×30.7 mm^2. (b) Magnified central area of (a), showing the pinned rotors and defining the parameters of the experiment (position, angle, and distance) described in the text. (c)–(f) Synchronization of two spiral rotors pinned to identical circular disks of diameters $d_1 = d_2 = 1.8$ mm and separated by a distance of $l = 4.68$ mm. The time evolutions of the (c) x and (d) y positional coordinates of rotors 1 (black circles) and 2 (red triangles) are shown. (e) Phase portrait of the x positions of the two rotors, with a black dashed line of slope -1. (f) Plot of y_1 versus y_2 (thick blue line with circles) showing in-phase synchronization. The corresponding x plot has been added in the background (in magenta) to show the emergence of mirror synchrony. The black and red dashed lines in (f) have slopes of -1 and $+1$, respectively.

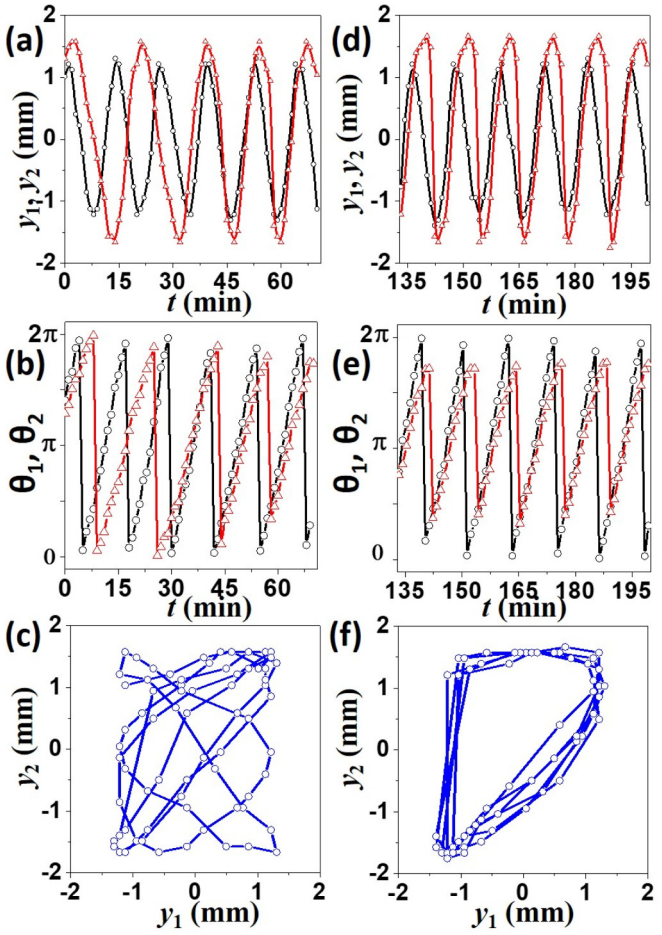

FIG. 2. Synchronization of two rotors having different initial frequencies. Here $d_1 = 1.8$ mm, $d_2 = 2.7$ mm, and $l = 12.15$ mm. Data from (a)–(c) the initial stage of the experiment and (d)–(f) the postsynchronization stage are depicted. (a) and (d) Time evolution of the y positions of the two rotors. (b) and (e) Plots of phase angles θ_1 and θ_2 versus time. (c) and (f) Phase portraits of the y coordinates. Black curves with circles are for the smaller rotor (rotor 1) and red curves with triangles are for the larger rotor (rotor 2) in (a)–(d). This coloring scheme is maintained throughout the paper for the time evolution of position (y_i) and angle (θ_i) coordinates.

An experiment using two identical disks is shown in Figs. 1(c)–1(f). Here both disks have diameters of 1.8 mm. The plots of x_i and y_i versus time are shown in Figs. 1(c) and 1(d), respectively. The two counterrotating spirals are placed side by side. Hence, if the initial phases of the two spirals are the same (i.e., $\theta_1 = \theta_2$ at $t = 0$), then the y coordinates of the tips will increase and decrease simultaneously, while the two x coordinates will have an opposing trend. The same is also observed in the phase plots shown in Figs. 1(e) and 1(f). This is an example of complete synchronization (in frequency and phase) between two counterrotating spirals. The y positions will be in-phase synchronized and the x positions out-of-phase synchronized. This is also called mirror synchronization [36] or mixed synchronization [15]. Since we maintain similar initial conditions in all our experiments and simulations, we compare only the y positions in all subsequent figures.

Figure 2 shows an example of synchronization between two spiral rotors, initially having different frequencies. The two spiral tips are pinned to disks of diameters $d_1 = 1.8$ mm and $d_2 = 2.7$ mm, with $l = 12.15$ mm. For the sake of convenience, henceforth we refer to the smaller obstacle as d_1 and the larger as d_2. Initially, the spiral pinned to the smaller disk [black curve in Fig. 2(a)] rotates faster than the other rotor ($T_1 \sim 12$ min and $T_2 \sim 18$ min). A plot of the phase angle with time is depicted in Fig. 2(b). It shows the incoherence in the rotational phase during the initial stages of oscillations. After several periods, it is observed that the two spirals rotate with the same frequency ($T \sim 12$ min). This is evident from the time plot of the y coordinate [Fig. 2(d)]. However, here the two rotors do not synchronize completely in-phase, but they have a slight lag. This is unlike the case of identical oscillators. A movie of this experiment (movie 2) can be found in the Supplemental Material [37]. The excitation wave emitted by a spiral rotor annihilates on touching another wave from a different spiral or target source. When both oscillators have an equal frequency, the wave arms emitted by them meet midway between the two rotors (at $l/2$) when they are initiated with almost the same phase. In the case of an initial mismatch of spiral frequencies, the waves emanated from the faster rotor (obstacle 1) gains over the slower one (obstacle 2). As it slowly invades the space of the second rotor, it accelerates it. Finally, when the waves from the smaller obstacle touches the larger obstacle, it generates a faster second rotor. So the frequency of rotor 2 is modified to match that of rotor 1. In this experiment, the time required for synchronization is around 58 min.

The phase diagram (y_1 versus y_2) of the two oscillators in the early part of the experiment fills the whole region [Fig. 2(c)]. This is expected due to the lack of frequency synchronization of the two rotors. In the later part of the experiment, we get a closed curve known as a Lissajous figure, which is a signature of frequency synchronization. However, the curve has a flat area around $y_1 = -1.3$ mm [Fig. 2(f)]. A close look at the position plot [Fig. 2(d)] will reveal a jump of oscillator 2 from $y_2 > 1.3$ to values of $y_2 < -1.3$ within two data points, recorded 1 min apart. This happens due to a phase resetting that occurs when the paths of the two oscillators cross. This interesting phenomenon is explained in more detail in Fig. 3. A close inspection of Fig. 2(b) shows a decreasing trend in the maximum value of θ_2 (red triangles). Upon synchronization, it can be observed that the phase angle of the larger rotor oscillates between 0.6π and 1.7π. This is also a manifestation of the phase resetting of the slower rotor by the faster one.

Figure 3 shows the wave-resetting dynamics around two rotors that differ more drastically in size ($d_1 = 1.8$ mm and $d_2 = 3.6$ mm). Four snapshots have been chosen at intervals of 3.2 min each, after synchronization has been reached. Once their frequencies have synchronized, the time required for the wave to complete one rotation around the larger obstacle has to match the time required to circulate around the smaller disk. As soon as the wave arm of the faster rotor touches the other heterogeneity, the phase angle of the latter is reset.

Here it is important to note the chirality of the two rotors. The larger rotor around d_2 rotates in a counterclockwise fashion and has negative chirality, while the smaller rotor around

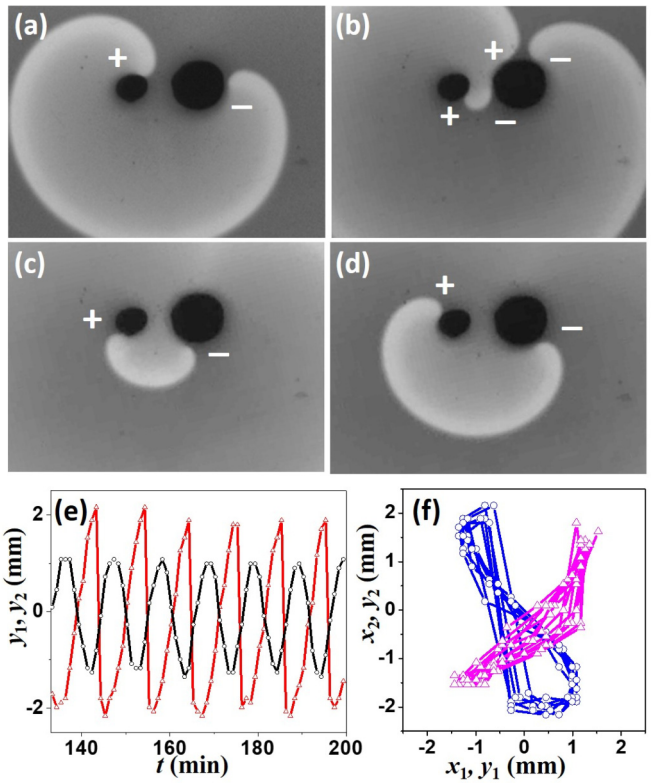

FIG. 3. Experiment depicting phase resetting during synchronization. The two rotors are pinned to unexcitable disks of diameters $d_1 = 1.8$ mm and $d_2 = 3.6$ mm and placed at a distance of $l = 4.86$ mm from each other. (a)–(d) Wave dynamics during phase resetting of the slower rotor (right) by the faster one. Snapshots were taken at (a) 114.8, (b) 118, (c) 121.2, and (d) 124.4 min, after the introduction of the pinning obstacles. The area of each snapshot is 23×17 mm^2. (e) Plots of the y position as a function of time, at a later stage of the experiment. (f) Phase plots of x_i (magenta triangles) and y_i (blue circles), showing mixed synchronization.

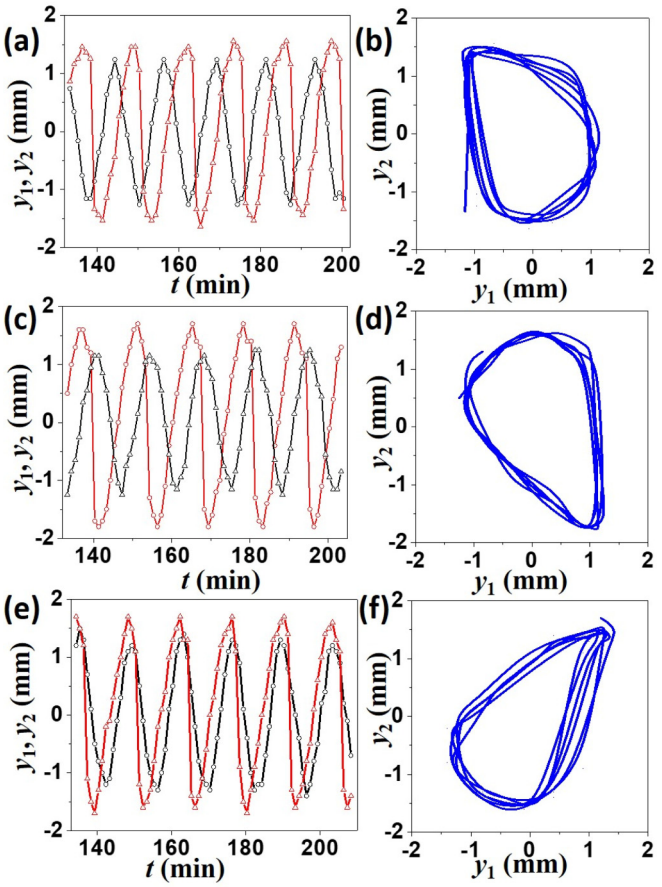

FIG. 4. Varying nature of synchronization with increasing interpin distance. Experiments with $d_1 = 1.8$ mm and $d_2 = 2.7$ mm are shown for (a) and (b) $l = 4.4$ mm, (c) and (d) $l = 8.15$ mm, and (e) and (f) $l = 10.7$ mm. (a), (c), and (e) Plots of the position coordinates with time, after synchronization has been reached. (b), (d), and (f) Relative positions of y_1 versus y_2, corresponding to the same time frame depicted in (a), (c), and (e), respectively.

d_1 rotates in a clockwise manner and can be said to have positive chirality [Fig. 3(a)]. As the spiral tips, now having the same speed, rotate around their individual pinning sites, the spiral around d_2 does not make a full round before the expanding wave from the first rotor touches the larger heterogeneity. The heterogeneity splits the wave, initiating a pair of spirals having opposite chirality on the second (larger) obstacle, both moving in opposite directions [Fig. 3(b)]. (Refer to movie 3 in the Supplemental Material for a more vivid display of the wave dynamics [37].) The newly formed positive spiral moves towards the original negative spiral on the obstacle, finally colliding with it and annihilating each other [Fig. 3(c)]. Its negative counterpart remains on the obstacle and continues its rotation until it comes across a newly formed positive spiral from the next colliding wave. So, for a very short time, there are actually three spiral tips on the larger obstacle [Fig. 3(b)].

The y-coordinate plot for the two spiral rotors, during the later stages of the experiment, after synchronization has been reached, are shown in Fig. 3(e). The value of y_2 plunges from its maximum to its minimum. These two positions correspond to the spiral tip at the top and bottom of disk 2, at times close to those in Figs. 3(b) and 3(c), respectively. Due to this sudden resetting of the phase of rotor 2 and its larger size, the two oscillators seemingly synchronize in an out-of-phase manner [Fig. 3(e)]. The phase portraits of x and y also support this idea [Fig. 3(f)]. The x and y plots still have opposing slopes, pointing towards mixed synchronization. However, they can no longer be said to be mirror synchronized, as the two rotors are no longer identical, and this is reflected in the difference of the x- and y-phase portraits, unlike what was seen in Fig. 1. Here the x plot is in-phase locked, while the y plot is out-of-phase locked [Fig. 3(f)]. This can be considered as an example of the interchange of rotational synchronization.

In order to explore the effect that the distance between the two rotors has on the synchronization behavior, we vary the l value between a set of two oscillators. Figure 4 shows a series of experiments with $d_1 = 1.8$ mm and $d_2 = 2.7$ mm and l values of 4.4, 8.15, and 10.7 mm. In every case, we observe frequency synchronization, after several rotations. The nature of phase synchronization is however slightly different in the three cases. They can phase lock in an almost-complete synchrony [Figs. 4(e) and 4(f)] or have a constant phase lag [Figs. 4(a)–4(d)]. While in the case of $l = 4.4$ mm [Figs. 4(a)

and 4(b)] we find that the phase resetting occurs at the beginning of the positive y_1 slope, near its minimum value, for $l = 8.15$ mm [Figs. 4(c) and 4(d)] it occurs at the end of the y_1 slope, near its maximum. Contrarily, for $l = 10.7$ mm [Figs. 4(e) and 4(f)] and for $l = 12.15$ mm [Figs. 2(d)–2(f)], phase jumps take place at the beginning and end of the decay of y_1, respectively. The increasing values of the interdisk distance l should be noted here.

IV. NUMERICAL MODEL

We choose the generic Barkley model for carrying out our numerical experiments. This model is widely used for the study of spiral and scroll waves in reaction-diffusion processes [38,39]. The two-variable model is given as

$$\frac{\partial u}{\partial t} = \frac{1}{\epsilon}\left[u(1-u)\left(u - \frac{v+b}{a}\right)\right] + D_u \nabla^2 u,$$
$$\frac{\partial v}{\partial t} = u - v + D_v \nabla^2 v,$$

where the activator u and inhibitor v are related to the concentrations of bromous acid and the oxidized form of ferroin, respectively; $D_u = D_v = 1.0$ are the diffusion coefficients of u and v, respectively; and $a = 0.84$, $b = 0.07$, and $\epsilon = 0.02$ are chosen as the system parameters. The space is discretized into 300×300 grid points and the system of equations is numerically integrated by using the fourth-order Runge Kutta method and a nine-point Laplace stencil. Zero-flux boundary conditions are applied across all four walls of the system. With a time interval of $\Delta t = 0.012$ (arbitrary time units) and step size $\Delta x = 0.35$ (arbitrary space units), this system can sustain rigidly rotating spiral waves having a core diameter of 1.8 space units, a wavelength of 18.2 space units, and a time period of 5.3 time units [25].

The numerical experiments are set up just like the BZ experiments. A plane wave is initiated between two unexcitable circular regions with diameters d_1 and d_2, placed at a distance l from each other. These act as pinning heterogeneities for the spiral waves. Throughout our simulations, we fix u and v within these circles at zero. A zero-flux boundary around these circular entities will not change the results of our simulations, except that the core size will be smaller in the latter case, leading to slightly reduced time periods. Initially, the variables u and v are taken to be zero across the entire space, except for a narrow region between the obstacles, where thin strips of altered values of the u and v variables are taken in a fashion so as to give directionality to the initial waveform [25]. With time, a pair of counterrotating spirals are eventually formed. The values of d_1, d_2, and l are varied to explore the dynamics of interacting pinned spiral rotors. We have taken obstacle diameters of 2.45, 3.85, 4.55, 5.25, and 5.95 space units, each having individual time periods of 4.9, 6.0, 6.6, 7.4, and 7.9 time units, respectively (for $d_1 = d_2$). The spiral tip is identified as the intersection of the isoconcentration lines $u = 0.5$ and $v = a/2 - b = 0.35$. Its coordinates with respect to the center of the spiral core are again labeled (x_i, y_i).

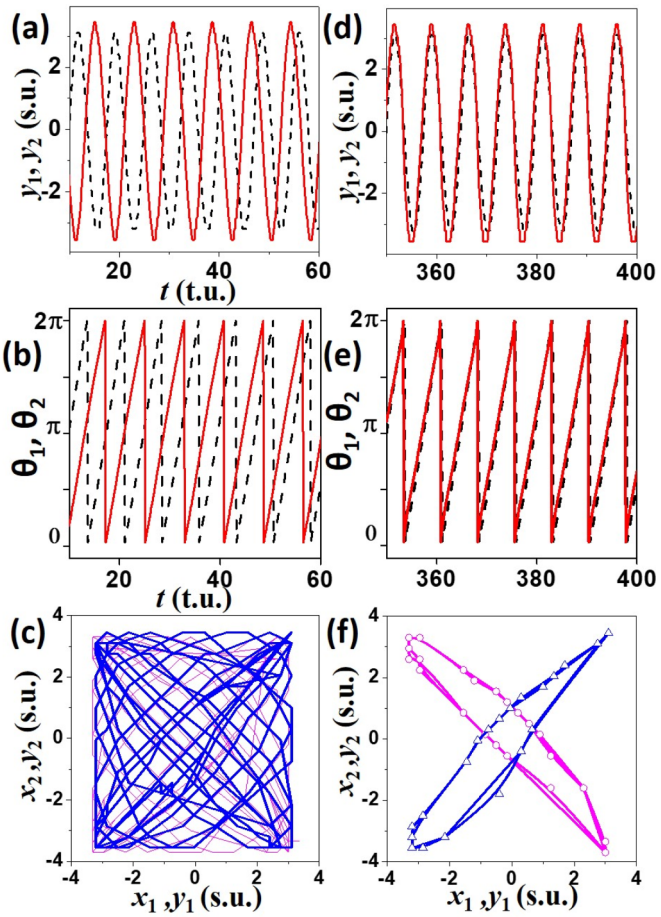

FIG. 5. In-phase synchronization of two spiral rotors for $d_1 = 5.25$, $d_2 = 5.95$, and $l = 40.95$. Simulation results are for (a)–(c) the initial and (d)–(f) postsynchronization stage of the study. (a) and (d) Variation of the vertical position y_i. (b) and (e) Phase angle variations with time. Black dashed lines are for rotor 1 and red solid lines are for rotor 2. (c) and (f) Phase plots of the two rotors. The y plots are blue curves with triangles, while the x plots are magenta curves with circles. A similar coloring scheme has been used in Fig. 6.

V. NUMERICAL RESULTS AND DISCUSSION

Figure 5 shows the synchronization of spiral rotors pinned to two disks of diameters $d_1 = 5.25$ and $d_2 = 5.95$ space units (s.u.), placed $l = 40.95$ space units apart. Initially, the two rotors oscillate with their individual time period, viz., 7.4 and 7.9 time units (t.u.), respectively. This is observable in Fig. 5(a), which also shows that the two oscillators are out of synchrony. After several rotations (over 40), the oscillators are seen to have synchronized perfectly in frequency. The time variation of the y coordinates of the spiral tips [Fig. 5(d)] bears testimony to the same. The time periods of both rotors are now 7.4 time units, the same as the characteristic frequency of the smaller obstacle (diameter 5.25). We observe similar trends across all combinations of pinning heterogeneities. The faster rotor always takes over the slower one and at the final stage the frequencies of the two rotors are the same. Observations along the same lines have been made in earlier studies of spiral waves [28,40]. Having established this, we now move on to

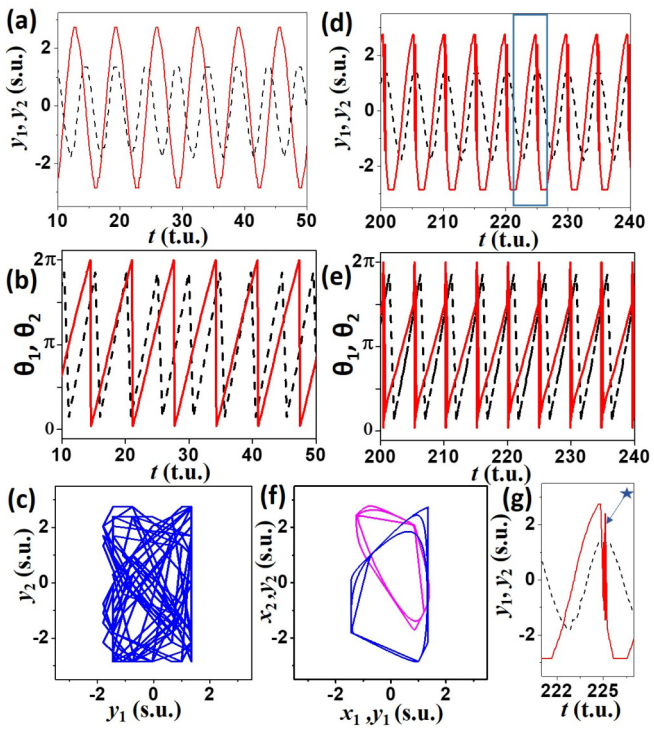

FIG. 6. Simulation result demonstrating phase jump and lag synchronization for disk diameters of $d_1 = 2.45$ and $d_2 = 4.55$ and the distance between the center of the disks $l = 110.95$: (a)–(c) initial results and (d)–(g) later results. Shown are (a) and (d) the dynamics of positional coordinates, (b) and (e) the phase angles, and (c) and (f) phase portraits demonstrating the emergence of lag synchronization. (g) Close-up of (d), showing the presence of multiple spiral tips on the second rotor (red solid curve) during phase resetting. The position is marked with a star.

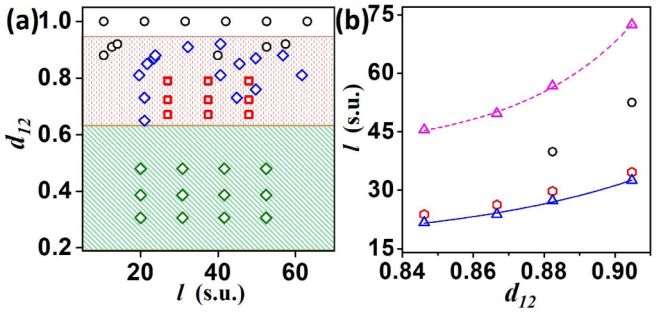

FIG. 7. Nature of synchronization as a function of interrotor distance l. (a) The ratio of the two diameters d_{12} $(=d_1/d_2)$ is plotted as a function of l. The green shaded area with diamonds depicts the phase-resetting dynamics and the red shaded area with squares shows lag synchronization. Blue triangles are points of antisynchronization (π-phase difference) and black circles denote points of complete synchronization (zero-phase difference). (b) Trend of in-phase and antiphase synchronization for a few d_{12} values. The blue solid line with triangles depicts the first occurrence of antiphase locking and magenta dashed line with triangles denotes the second occurrence of antisynchronization, as l is increased. Black circles denote any in-phase synchronized state between these two lines. The red hexagons stand for the wavelength of the faster spiral (λ_1).

explore the phase dynamics of the frequency-synchronized rotors.

The phase angles θ_1 and θ_2 plotted in Fig. 5(b) show that initially the rotors are not phase synchronized. The space-filling plot of y_1 versus y_2 [Fig. 5(c)] also confirms the asynchronous behavior of the two rotors in the early stages of the experiment. The exact overlap of θ_1 and θ_2 at later times in Fig. 5(e) confirms the in-phase locking synchronization of the two rotors. The phase portrait for y_1 versus y_2 (x_1 versus x_2) in Fig. 5(f) is a thin ellipse along the right (left) diagonal, which establishes that the two counterrotating spirals are synchronized in phase.

This kind of exact phase locking was not observed for our experiments having rotors of different initial frequencies. Additional simulations confirmed that such strong synchronization would only be possible for pinning sizes of comparable dimensions. Otherwise, the mismatch in the size leads to the phase resetting phenomenon, which will not allow the y-positional coordinates to match exactly throughout one oscillation. More experiments have to be carried out for the BZ system with pinning disk sizes that vary about 10% in diameter in order to be able to observe complete phase synchrony.

In Fig. 6 we show the synchronization of two rotors pinned around heterogeneities of extensively different diameters, viz., $d_1 = 2.45$ and $d_2 = 4.55$ space units. The initial data show the unsynchronized nature of the two oscillators [Figs. 6(a)–6(c)]. After frequency synchronization, the two rotors are seen to display a unique dynamics in both position and angle. Here the phase jump of the larger rotor (red solid lines) is evident in the plots of position as well as phase angle [Figs. 6(d) and 6(e)]. The plot of y_1 versus y_2 shows a wide elliptic profile which is typical of two oscillators having equal frequencies and a constant phase shift [Fig. 6(f)]. Hence we might call it a case of lag synchrony.

In Fig. 3 the experimental snapshots have shown the presence of three spiral tips on the larger obstacle, for a very short time (compared to time period). The signature of the new singularities are observable in the plot of the y coordinate of the tip (y_2), as well as the corresponding phase angle (θ_2) plot [Figs. 6(d) and 6(e)]. A small portion of Fig. 6(d) is expanded at Fig. 6(g) for better visibility. At the instant of the overlap of the two tip positions [marked with a blue star around 225 time units in Fig. 6(g)], there is more than one spiral tip identified by our program. Subsequently, the phase position and angle are reset as a result of this intricate dynamics. The phase portraits at later times [Fig. 6(f)] have the flattened ellipse structure seen in Figs. 2 and 4.

A phase diagram for studying the nature of synchronization has been constructed. Figure 7 depicts the changing dynamics of the interacting rotors as a function of the ratio of obstacle diameter (d_{12}) and the space separating them, l. When the two obstacles are of widely differing dimensions ($d_{12} < 0.65$), we observe phase-resetting dynamics [Fig. 7(a)]. As the ratio increases, we move to a region of lag synchronization. Within this region we come across some points of antiphase synchronization and fewer points of complete in-phase locking. A deeper analysis of these seemingly arbitrary points reveals that the first antiphase synchronization for a given ratio occurs at the value of $l \simeq \lambda_1 - d_s$, where λ_1 is the wavelength of

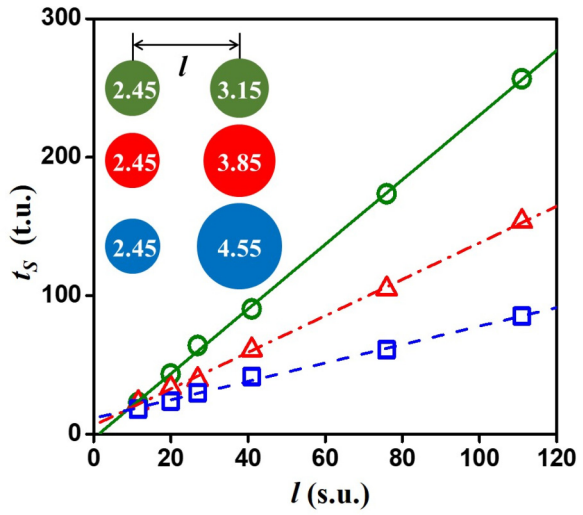

FIG. 8. Variation of synchronization time t_S with increasing interrotor distances l, for three sets of obstacle sizes. $d_1 = 2.45$ space units across all simulations. The d_2 values are 3.15 (olive circles), 3.85 (red triangles), and 4.55 (blue squares) across the three graphs.

the spiral wave arm near the smaller obstacle and d_s is the core diameter of a free spiral [Fig. 7(b)]. This is an interesting observation when seen in the context of interacting spiral waves. It has been established in a recent study on the interaction of free spirals that two spiral cores having the same frequency cannot modify the trajectory of one another when placed beyond a critical distance d_c, where $d_c = \lambda - d_s$ [25] (here λ is the characteristic wavelength of the spiral). This critical distance is close to the l value showing the first antiphase synchronization of nonidentical rotors in Fig. 7(b). The second antiphase synchronization occurs after a larger distance. At ratios greater than 0.88, complete synchronization occurs at some specific values of l, which lie between the two antiphase synchronized states. At $d_{12} = 1.0$, or obstacles of equal diameter, in-phase synchronization is observed for all values of l. While in the numerical simulations we are able to initiate waves with the exact same phase of rotation, this is not always the case in experiments. There the initial phases of the two spirals may be the same or different. In simulations with rotors of the same initial frequency (attached to identical circular disks) having different initial phases, we found that the spirals synchronize in phase as long as they are within one wavelength of each other. Beyond that distance ($l > \lambda_1$), the two rotors are locked with the initial phase lag. This can be explained on the basis of the fact that when the frequencies of both waves are equal, the wave arms touch each other somewhere between the heterogeneities, and if this distance is more than the critical distance d_c, one spiral will not be able to modify the phase of the other [25].

We also measured the time required for synchronization (t_S) for varying obstacle sizes and spacings. Figure 8 shows the variation of t_S as a function of the distance between the two rotors, l, for three sets of d_2 values. We have kept d_1 constant at 2.45 space units. We see that for a given d_2 value, t_S increases linearly with l. The velocity of the waves emanated by rotor1 remains the same for all the experiments. As the distance between the two rotors increases, the time required for the waves to cover this path and reach the slower rotor increases, which is reflected in the positive slopes of the lines. However, with the increase in the value of d_2, the time of synchronization decreases. This happens because, as we increase the size of the heterogeneity (d_2), the rotor becomes slower. The number of waves it emits in some given time also decreases. Hence, the wave arm of the faster rotor has to overcome fewer collisions with the oncoming waves. This enables it to reach the second rotor within a shorter time duration, thus leading to smaller t_S values. For a given l, t_S is smallest for the largest d_2 value, except when $l < \lambda$, when all values of t_S are almost comparable. Within one wavelength, the wave arm of the faster rotor does not have to encounter any oncoming waves from its larger neighbor, before reaching it. (Refer to movie 4 in [37] for an example of such wave activity.) The slope of the graph for the smallest obstacle 2 size (d_2) is the highest, meaning that the farther apart the two beads are placed, the longer it will take for the waves from obstacle 1 to reach obstacle 2 and also it has to encounter more oncoming waves. So these two factors contribute to an increase in the slope of the line.

Similar trends are observable for our experimental results. In general, the time of synchronization increases with increasing distance between a set of rotors. We carried out several experiments with exactly the same circular disks of diameters $d_1 = 1.8$ mm and $d_2 = 2.7$ mm (some of which are depicted in Figs. 2 and 3). The trend of synchronization time with distance was linear. A plot of t_S versus l for this set of heterogeneities can be found in the Supplemental Material (Fig. S1 [37]). Some points are found to deviate a little from the straight line, which may be because of several factors such as temperature fluctuation or air bubbles leading to slight local heterogeneities.

VI. CONCLUSION

We have established that a system of pinned spiral waves can be considered to be a promising candidate for the study of rotational synchronization. It will be an addition to the already existing library of rotors such as Josephson junctions, mechanical rotors, and camphor boats used for such studies. We have shown with our experiments and simulations that spiral rotors pinned to unexcitable heterogeneities can indeed act as coupled oscillators that synchronize in frequency and phase. By pinning the spirals to disks of different dimensions, we were able to generate and sustain spirals of different characteristic frequencies while also ensuring that they do not translate in space. With that ensured, we carried out detailed observations of rotor position and phase angle to show how two initially unsynchronized rotors with different frequencies and sometimes phase can synchronize. Depending on several factors, such as a difference in obstacle size and the distance separating them, we observed in-phase locking, out-of-phase locking, lag synchronization, and phase resetting. The results of our numerical simulations have corroborated the different kinds of phenomena observed in our experiments while illustrating the nuances of phase resetting in the larger obstacle. Also, a linear trend in the synchronization times with interrotor distance has been established. This may be explored

in future investigations to obtain an estimate of the coupling strength of these pinned rotors.

The chirality of the two spiral rotors play an important role in their interaction. It will be interesting to study experimentally the interaction of corotating pinned spiral waves. Future investigations could be carried out with lattices of spiral rotors. As established for free spirals [25], the nature of the interaction of pinned spirals may also change with an increased number of coupled rotors, which may give rise to a plethora of richer synchronization dynamics.

In the cardiac system, the pinning of free spiral waves is known to modify polymorphic ventricular tachycardia into a monomorphic one [4]. If there is more than one such pinned excitation wave, their interaction may change the nature of the graph obtained from an electrocardiogram (ECG), which is commonly used to monitor cardiac activity in patients. Studies of wave propagation dynamics in the cardiac system suggest that the activity of a high-frequency rotor can give rise to the fastest dominant frequency domain [41]. Hence a better understanding of wave interaction and synchronization will be of vital importance in a correct diagnosis of heart conditions based on clinical procedures, such as the use of ECG.

ACKNOWLEDGMENTS

This work was partially supported by the Science and Engineering Research Board, Government of India (Grant No. CRG/2019/001303). Thanks are due to Dr. Nirmali Prabha Das for helpful discussions.

[1] A. Pikovsky, M. Rosenblum, and J. Kurths, *Synchronization* (Cambridge University Press, Cambridge, 2003).
[2] B. Blasius, A. Huppert, and L. Stone, Nature (London) **399**, 354 (1999).
[3] V. Hakim and N. Brunel, Neural Comput. **11**, 1621 (1999).
[4] J. Jalife, M. Delmar, J. Anumonwo, O. Berenfeld, and J. Kalifa, *Basic Cardiac Electrophysiology for the Clinician*, 2nd ed. (Wiley-Blackwell, Oxford, 2009).
[5] M. Bier, B. M. Bakker, and H. V. Westerhoff, Biophys. J. **78**, 1087 (2000).
[6] A. Biswas, D. Das, and P. Parmananda, Phys. Rev. E **95**, 042202 (2017).
[7] R. Toth, A. F. Taylor, and M. R. Tinsley, J. Phys. Chem. B **110**, 10170 (2006).
[8] Y. Kuramoto, *Chemical Oscillations, Waves, and Turbulence* (Springer, Berlin, 1984).
[9] B. C. Daniels, S. T. M. Dissanayake, and B. R. Trees, Phys. Rev. E **67**, 026216 (2003).
[10] J. Sharma, I. Tiwari, D. Das, V. Pimienta, and P. Parmananda, Phys. Rev. E **101**, 052202 (2020).
[11] I. I. Blekhman, *Synchronization in Science and Technology* (ASME, New York, 1988).
[12] J. Schwarz-Linek, C. Valeriani, A. Cacciuto, M. E. Cates, D. Marenduzzo, A. N. Morozov, and W. C. K. Poon, Proc. Natl. Acad. Sci. U.S.A. **109**, 4052 (2012).
[13] R. Di Leonardo, A. Búzás, L. Kelemen, G. Vizsnyiczai, L. Oroszi, and P. Ormos, Phys. Rev. Lett. **109**, 034104 (2012).
[14] J. Sharma, I. Tiwari, D. Das, P. Parmananda, V. S. Akella, and V. Pimienta, Phys. Rev. E **99**, 012204 (2019).
[15] A. Prasad, Chaos Soliton. Fract. **43**, 42 (2010).
[16] J. Sharma, I. Tiwari, D. Das, and P. Parmananda, Phys. Rev. E **103**, 012214 (2021).
[17] E. Pálsson, K. J. Lee, R. E. Goldstein, J. Franke, R. H. Kessin, and E. C. Cox, Proc. Natl. Acad. Sci. U.S.A. **94**, 13719 (1997).
[18] Y. Yu, L. M. Santos, L. A. Mattiace, M. L. Costa, L. C. Ferreira, K. Benabou, A. H. Kim, J. Abrahams, M. V. L. Bennett, and R. Rozental, Proc. Natl. Acad. Sci. U.S.A. **109**, 2585 (2012).
[19] R. Singh, J. Xu, N. G. Garnier, A. Pumir, and S. Sinha, Phys. Rev. Lett. **108**, 068102 (2012).
[20] X. Huang, W. Xu, J. Liang, K. Takagaki, X. Gao, and J.-Y. Wu, Neuron **68**, 978 (2010).
[21] E. M. Cherry and F. H. Fenton, New J. Phys. **10**, 125016 (2008).
[22] S. Jakubith, H. H. Rotermund, W. Engel, A. von Oertzen, and G. Ertl, Phys. Rev. Lett. **65**, 3013 (1990).
[23] A. T. Winfree, Science **175**, 634 (1972).
[24] D. Mahanta, N. P. Das, and S. Dutta, Phys. Rev. E **97**, 022206 (2018).
[25] H. Kalita and S. Dutta, Phys. Rev. E **105**, 054213 (2022).
[26] E. A. Ermakova, A. M. Pertsov, and E. E. Shnol, Physica D **40**, 185 (1989).
[27] S. Dutta and O. Steinbock, Phys. Rev. E **83**, 056213 (2011).
[28] V. Krinsky and K. Agladze, Physica D **8**, 50 (1983).
[29] O. Steinbock and S. C. Müller, Phys. Rev. E **47**, 1506 (1993).
[30] J. Jalife, R. A. Gray, G. E. Morley, and J. M. Davidenko, Chaos **8**, 79 (1998).
[31] F. Xie, Z. Qu, and A. Garfinkel, Phys. Rev. E **58**, 6355 (1998).
[32] D. Olmos, Phys. Rev. E **81**, 041924 (2010).
[33] W.-J. Rappel, Phys. Rev. E **105**, 014404 (2022).
[34] M. Sutthiopad, J. Luengviriya, P. Porjai, M. Phantu, J. Kanchanawarin, S. C. Müller, and C. Luengviriya, Phys. Rev. E **91**, 052912 (2015).
[35] F. M. Zanotto and O. Steinbock, Phys. Rev. E **103**, 022213 (2021).
[36] K. Czolczynski, P. Perlikowski, A. Stefanski, and T. Kapitaniak, Commun. Nonlinear Sci. Numer. Simulat. **17**, 3658 (2012).
[37] See Supplemental Material at http://link.aps.org/supplemental/10.1103/PhysRevE.106.034201 for a figure showing the linear trend of synchronization time for our experiments (Fig. S1) and movies corresponding to Figs. 2, 3, 4(a), 5, and 6.
[38] D. Barkley, M. Kness, and L. S. Tuckerman, Phys. Rev. A **42**, 2489 (1990).
[39] D. Barkley, Physica D **49**, 61 (1991).
[40] U. Parlitz, A. Schlemmer, and S. Luther, Phys. Rev. E **83**, 057201 (2011).
[41] F. H. Samie and J. Jalife, Cardiovasc. Res. **50**, 242 (2001).